Broadband Fixed Phase Shifters

Amin M. Abbosh, *Senior Member, IEEE*

***Abstract*—A method to design planar and compact phase shifters with broadband characteristics is presented. It utilizes broadside-coupled microstrip-coplanar waveguide, and thus the proposed devices can be fabricated using the simple and cheap double-side printed circuit boards. The method is used to design 60° and 90° phase shifters. The simulated and measured results show that the developed phase shifters achieve 3 to 11 GHz bandwidth with low phase instability ($\pm 2°$), very low insertion loss (0.4 dB), high return loss (15 dB), and a compact size ($1.5\ \text{cm} \times 2\ \text{cm}$).**

***Index Terms*—Coupled transmission lines, electromagnetic coupling, phase Shifters, planar transmission lines.**

I. Introduction

PHASE shifters are key devices in many microwave systems, such as intelligent antennas, microwave instrumentations, modulators, to name a few.

The conventional approach to design planar phase shifters is to use the Schiffman differential phase shifter or one of its variations that rely on the edge-coupled transmission lines [1]. However, a very narrow gap between the edge-coupled lines is needed for a broadband performance.

In an important development, multilayer broadside-coupled structures were utilized to build ultra-wideband (UWB) phase shifters with excellent performance [2]. This multilayer phase shifter has recently been utilized to build UWB Butler matrix for switched beam antenna array that operates across the range 3.1 to 10.6 GHz [3]. However, the multilayer configuration is not the preferred option for some applications which require the use of the simple and low-cost printed circuit board (PCB) technology. Moreover, the multilayer structure could pose some manufacturing challenges as any error in the alignment of the different layers may cause a significant degradation in the performance.

In recent developments, reflective-, active-, liquid crystal polymer-, metamaterials-, and substrate integrated waveguide-based phase shifters are proposed [4]–[10]. However, all of those types have either a limited relative bandwidth (10%-40%) or a high insertion loss (2 to 5 dB), in addition to their complicated and costly manufacturing process.

In this letter, a broadside-coupled microstrip-coplanar waveguide (CPW) structure is utilized to develop broadband phase shifters. The proposed approach enables the use of PCB to develop phase shifters with low phase variation ($\approx \pm 2°$), very low insertion loss ($\approx$ 0.4 dB), and high return loss ($\approx$ 15 dB).

Manuscript received June 09, 2010; revised August 09, 2010; accepted September 14, 2010. Date of publication November 29, 2010; date of current version January 07, 2011. This work was supported by the ARC Future Fellowship, Australia.

The author is with the School of ITEE, The University of Queensland, QLD 4072, Australia (e-mail: a.abbosh@uq.edu.au).

Color versions of one or more of the figures in this letter are available online at http://ieeexplore.ieee.org.

Digital Object Identifier 10.1109/LMWC.2010.2079320

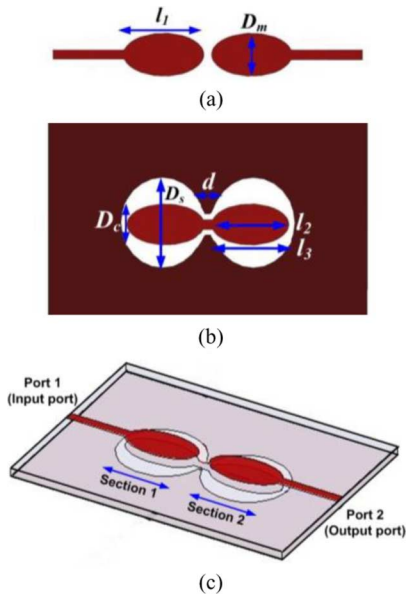

Fig. 1. Proposed structure of the phase shifter. (a) Top layer. (b) Bottom layer. (c) Side view of the whole structure.

II. Proposed Device

The configuration of the proposed phase shifter is shown in Fig. 1. It can be classified as a two-section broadside-coupled microstrip-CPW structure. Those two sections are connected together via a short length of CPW in the bottom layer. Two sections are used to achieve a uniplanar structure (input and output ports at the same layer) with one form of transmission lines, and to increase the range of the achievable phase shift. The elliptical shape for the coupled structure depicted in Fig. 1 is used because of its ability to achieve an almost constant coupling factor over a wide band [2].

Following the analysis of the multisection coupled structures [11], it is possible to show that the effective scattering parameters for the two-section broadside-coupled structure ($S_{11\text{ef}}$ and $S_{21\text{ef}}$) shown in Fig. 1(c) are given as

$$S_{11\text{ef}} = S_{11} + \frac{S_{21}^2 S_{11}}{1 - S_{11}^2};\ S_{21\text{ef}} = \frac{S_{21}^2}{1 - S_{11}^2} \tag{1a}$$

$$S_{11} = \frac{1 - CF^2\left(1 + \sin^2(\beta_{\text{ef}} l_3)\right)}{\left[\sqrt{1 - CF^2}\cos(\beta_{\text{ef}} l_3) + j\sin(\beta_{\text{ef}} l_3)\right]^2} \tag{1b}$$

$$S_{21} = \frac{j2CF\sqrt{1 - CF^2}\sin(\beta_{\text{ef}} l_3)}{\left[\sqrt{1 - CF^2}\cos(\beta_{\text{ef}} l_3) + j\sin(\beta_{\text{ef}} l_3)\right]^2} \tag{1c}$$

where S_{11} and S_{21} are the scattering parameters for one section of the coupled structure, CF is the coupling factor between the top and bottom layer of a one-section broadside-coupled structure, β_{ef} is the effective phase constant in the medium of the coupled structure, and l_3 is the physical length of the coupled structure.

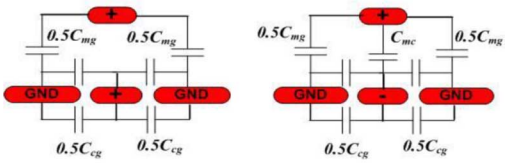

(a) (b)

Fig. 2. Capacitances of the used structure for the two modes of operation. (a) C-mode (b)π-mode.

If the device is designed properly such that $S_{11} = 0$, the differential phase shift ($\Delta\Phi$) of the output signal compared to a normal microstrip transmission line of length l_m and phase constant β_m can be found from (1a)–(1c)

$$\Delta\Phi = 180^\circ - 4\arctan\left[\frac{\sin(\beta_{\text{ef}} l_3)}{\sqrt{1-CF^2}\cos(\beta_{\text{ef}} l_3)}\right] + \beta_m l_m. \quad (2)$$

The main reason behind the possibility of achieving a constant $\Delta\Phi$ as given in (2) across the UWB is the constant CF of the utilized structure across that band. The effect of the variation in $\beta_{\text{ef}} l_3$ with frequency can be compensated by the reverse effect of $\beta_m l_m$. This step requires the optimization of l_m for a minimum deviation in $\Delta\Phi$ across the UWB.

Following the analysis presented in [2], it is possible to show using (2) that, for a UWB performance, the proposed structure can achieve a phase shift across the range from 30° to 90°. The coupling factor CF is the parameter that can be used to control value of the differential phase shift. After calculating the value of CF needed to achieve the required phase shift from (2), the physical dimensions for the structure are to be found. Thus, the relation between the coupling factor CF and the physical dimensions of each section of the device shown in Fig. 1 needs to be derived.

The structure depicted in Fig. 1 can be analyzed using the C-and π-mode approach. For the C-mode, the two layers are excited in-phase, whereas in the π-mode, the top and bottom layers are out-of-phase with respect to the ground.

Assuming a quasi transverse electromagnetic propagation, the electrical characteristics of the coupled lines can be completely determined from the effective capacitances per unit length of the lines and the phase velocity on the lines [11]. Therefore, the structures shown in Fig. 2 can be used to analyze the proposed device.

For each of the two modes of propagation, the capacitance for each of the two coupled lines can be determined from Fig. 2. The C-mode capacitance for the microstrip (C_{me}) and the CPW(C_{ce}) are equal to

$$C_{me} = C_{mg}; C_{ce} = C_{cg}. \quad (3a)$$

The π-mode capacitance for the microstrip (C_{mo}) and the CPW(C_{co}) are equal to

$$C_{mo} = C_{mg} + 2C_{mc}; C_{co} = C_{cg} + 2C_{mc}. \quad (3b)$$

Using the quasi-static approach with the help of the conformal mapping technique, the capacitances shown in Fig. 2 can be calculated as a function of the coupled structure's dimension

$$C_{mg} = 2\varepsilon_o\varepsilon_r\frac{K'(k_1)}{K(k_1)}; C_{cg} = 2\varepsilon_o\left[(\varepsilon_r - 1)\frac{K(k_2)}{K'(k_2)} + 2\frac{K(k_3)}{K'(k_3)}\right] \quad (4a)$$

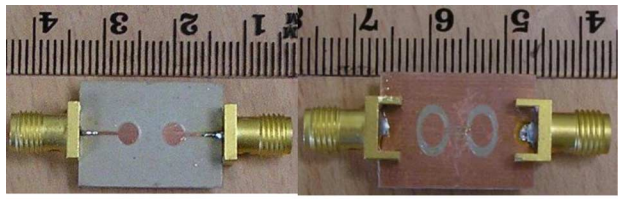

(a) (b)

Fig. 3. (a) Top and (b) bottom view of the developed 60° phase shifter.

$$C_{mc} = \varepsilon_o\varepsilon_r\frac{D_m + D_c}{2h} \quad (4b)$$

$$k_1 = \frac{\sinh\left(\frac{\pi D_s}{(4h)}\right)}{\sqrt{\sinh^2\left(\frac{\pi D_s}{(4h)}\right) + \cosh^2\left(\frac{\pi D_m}{(4h)}\right)}} \quad (4c)$$

$$k_2 = \frac{\sinh\left(\frac{\pi D_c}{(4h)}\right)}{\sinh\left(\frac{\pi D_s}{(4h)}\right)}; k_3 = \frac{D_c}{D_s} \quad (4d)$$

$K(k)$ and $K'(k)$ are the first kind elliptical integral and its complementary, respectively, D_m, D_c, and D_s are the diameters shown in Fig. 2, and h is the thickness of the substrate.

The characteristic impedance of each of the two lines (microstrip at the top layer and CPW at the bottom layer) at any of the two modes can be found as follows [10]:

$$Z_{ij} = \sqrt{\frac{\varepsilon_r}{(c_o C_{ij})}}. \quad (5)$$

The subscript i refers to the line (m for microstrip and c for CPW) and j refers to the mode (e for C-mode and o for π-mode), c_o is velocity of light in free space, and ε_r is the dielectric constant of the substrate.

The structure shown in Figs. 1 and 2 is asymmetrical. Therefore, the analysis approach for asymmetrical broadside-coupled lines is used [12]. Hence, it is possible to find the coupling factor between the top layer and the bottom layer (CF) using the following equation [12]:

$$CF = \sqrt{\frac{Z_{me}Z_{mo}}{Z_{ce}Z_{co}}}\frac{Z_{ce} - Z_{co}}{\sqrt{(Z_{me} + Z_{mo})(Z_{ce} + Z_{co})}}. \quad (6)$$

For a perfect matching between the coupled structure and the input/output ports, which have characteristic impedance $Z_o (= 50\,\Omega)$, the C-and π-mode impedances of the coupled microstrip patches should satisfy the following relation [12]:

$$Z_o = \sqrt{Z_{me}Z_{mo}}. \quad (7)$$

The coupling factors as a function of the capacitances can be obtained by substituting from (3) and (5) into (6). The design (4)–(6) can now be used to find the initial dimensions (D_m, D_c, and D_s) of the device.

Concerning lengths of the coupled structure (l_1 and l_3), they are initially chosen to be equal to quarter of the effective wavelength at the centre of the passband (6.85 GHz). The length l_2 is less than l_3 by the value of the narrow slot needed in the ground plane to form the CPW.

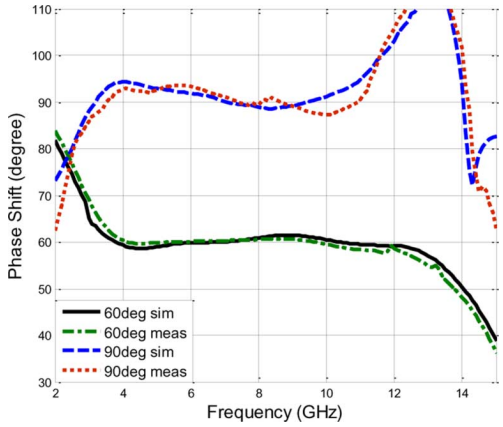

Fig. 4. Phase performance of the designed devices.

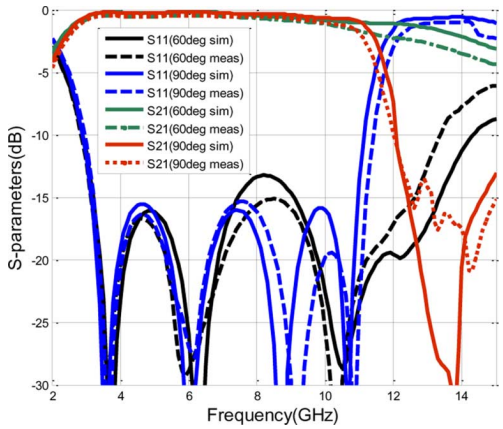

Fig. 5. S-parameters of the designed devices.

III. Results

To test the performance of the proposed device, 60° and 90° phase shifters were designed and fabricated using Rogers RT6010 ($\varepsilon_r = 10.2$, $h = 0.635$ mm) as the substrate. The proposed design method was used to calculate the initial dimensions of the devices, whereas the final dimensions were found using the optimization capability of the software HFSS. It was noted that the absolute difference between the initial and the optimized values is less than 12% reflecting the accuracy of the utilized theoretical analysis.

The optimized dimensions in (mm) are $D_m = 3.18$, $D_c = 4.36$, $D_s = 6.82$, $l_1 = 3.02$, $l_2 = 3$, and $l_3 = 4.02$ for the 60° device, and $D_m = 1.88$, $D_c = 3.64$, $D_s = 5.8$, $l_1 = 4.06$, $l_2 = 4.14$, and $l_3 = 4.96$ for the 90° device. The distance d has no significant impact on the performance, and for a compact structure, it is chosen to be as small as possible; $d = 1.3$ mm for the 60° device, and 1.03 mm for the 90° device. Size of the devices excluding the reference line is $1.5\text{cm} \times 2$ cm. A photo of one of the developed devices is shown in Fig. 3.

The performance of the designed devices was verified using the software HFSS and then measured using a vector network analyzer. The simulated and measured $\Delta\Phi$ of the 60°, and 90° phase shifters are shown in Fig. 4. The value of $\Delta\Phi$ is $60° \pm 1°$ in the simulations and $60° \pm 2°$ according to the measured results for the 60° phase shifter across the band from 3.5 to 12 GHz. It is interesting to see from Fig. 4 that the achieved phase shift of this device is almost constant at 60° across the band from 4 GHz to more than 12 GHz. For the 90° phase shifter, $\Delta\Phi$ is $90° \pm 3°$ for the band 3 to 11 GHz.

The S-parameters of the developed devices are shown in Fig. 5, which reveals a passband of 2.8 GHz to more than 12 GHz for the 60° phase shifter and 2.8 to 11 GHz for the 90° phase shifter assuming the 10 dB return loss as a reference. The insertion losses of the two phase shifters are less than 0.2 dB in the simulations and less than 0.4 dB in the measurements across those passbands. Fig. 5 also shows that the return losses of the two developed phase shifters are more than 15 dB across most of the passbands.

The performance of the developed devices is also tested when connected as a complete differential phase shifter using two single-pole double-throw switches. It was noted that the phase performance and the return loss are exactly as shown in Figs. 4 and 5, whereas the insertion losses increase by 0.45 dB due to the use of those switches as proven by their technical specifications.

IV. Conclusion

A broadband phase shifter that can achieve a constant differential phase has been presented. The device utilizes a broadside-coupled microstrip-CPW structure, which enables a simple and cheap manufacturing process using the printed circuit board's technology. A complete design procedure has been presented for the proposed device that has a compact size of $1.5\,\text{cm} \times 2\,\text{cm}$. The simulated and measured results of the developed 60°, and 90° phase shifters have shown 3 to 11 GHz bandwidth.

References

[1] Y. Guo, Z. Zhang, and L. Ong, "Improved wide-band Schiffman phase shifter," *IEEE Trans. Microw. Theory Tech.*, vol. 54, no. 3, pp. 1196–1200, Mar. 2006.

[2] A. Abbosh, "Ultra-wideband phase shifters," *IEEE Trans. Microw. Theory Tech.*, vol. 55, no. 9, pp. 1935–1941, Sep. 2007.

[3] S. Ibrahim and M. Bialkowski, "Wideband butler matrix in microstrip-slot technology," in *Proc. Asia-Pacific Microw. Conf.*, Singapore, 2009, pp. 2104–2107.

[4] K. Sellal, L. Talbi, T. A. Denidni, and J. Lebel, "Design and implementation of a substrate integrated waveguide phase shifter," *IET Microw. Antennas Propag.*, vol. 2, no. 2, pp. 194–199, 2008.

[5] Y. J. Cheng, W. Hong, and K. Wu, "Millimeter-wave multibeam antenna based on eight-port hybrid," *IEEE Microw. Wireless Compon. Lett.*, vol. 19, no. 4, pp. 212–214, Apr. 2009.

[6] Y. Cheng, W. Hong, and K. Wu, "Broadband self-compensating phase shifter combining delay line and equal-length unequal-width phaser," *IEEE Trans. Microw. Theory Tech.*, vol. 58, no. 1, pp. 203–210, Jan. 2010.

[7] C. Lin, S. Chang, and W. Hsiao, "A full-360 reflection-type phase shifter with constant insertion loss," *IEEE Microw. Wireless Compon. Lett.*, vol. 18, no. 2, pp. 106–108, Mar. 2008.

[8] M. Hangai, M. Hieda, N. Yunoue, Y. Sasaki, and M. Miyazaki, "S-and C band ultra-compact phase shifters based on all-pass networks," *IEEE Trans. Microw. Theory Tech.*, vol. 58, no. 1, pp. 41–47, Jan. 2010.

[9] F. Goelden, A. Gaebler, M. Goebel, A. Manabe, S. Mueller, and R. Jakoby, "Tunable liquid crystal phase shifter for microwave frequencies," *Electron. Lett.*, vol. 45, no. 13, pp. 686–687, 2009.

[10] P. He, J. Gao, C. Marinis, P. Parimi, C. Vittoria, and V. Harris, "A microstrip tunable negative refractive index metamaterial and phase shifter," *Appl. Phys. Lett.*, vol. 93, no. 19, pp. 193505-1–193505-3, 2008.

[11] A. Abbosh, "Planar bandpass filters for ultra wideband applications," *IEEE Trans. Microw. Theory Tech.*, vol. 55, no. 10, pp. 2262–2269, Oct. 2007.

[12] A. Abbosh, "Design of ultra-wideband three-way arbitrary power dividers," *IEEE Trans. Microw. Theory Tech.*, vol. 56, no. 1, pp. 194–201, Jan. 2008.